Neurotherapeutics (2021) 18:1095–1112
https://doi.org/10.1007/s13311-021-01015-8

ORIGINAL ARTICLE

Targeting TDP-43 Pathology Alleviates Cognitive and Motor Deficits Caused by Chronic Cerebral Hypoperfusion

Sai Sampath Thammisetty[1,4] · Laurence Renaud[1] · Vincent Picher-Martel[1,3] · Yuan Cheng Weng[1] · Frédéric Calon[3,4] · Stephan Saikali[2,3] · Jean-Pierre Julien[1,5] · Jasna Kriz[1,5]

Accepted: 22 January 2021 / Published online: 30 March 2021

Abstract

Vascular dementia is one of the most common forms of dementia in aging population. However, the molecular mechanisms involved in development of disease and the link between the cerebrovascular pathology and the cognitive impairments remain elusive. Currently, one common and/or converging neuropathological pathway leading to dementia is the mislocalization and altered functionality of the TDP-43. We recently demonstrated that brain ischemia triggers an age-dependent deregulation of TDP-43 that was associated with exacerbated neurodegeneration. Here, we report that chronic cerebral hypoperfusion in mice (CCH) produced by unilateral common carotid artery occlusion induces cytoplasmic mislocalization of TDP-43 and formation of insoluble phosho-TDP-43 aggregates reminiscent of pathological changes detected in cortical neurons of human brain samples from patients suffering from vascular dementia. Moreover, the CCH in mice caused chronic activation of microglia and innate immune response, development of cognitive deficits, and motor impairments. Oral administration of a novel analog (IMS-088) of withaferin A, an antagonist of nuclear factor-κB essential modulator (NEMO), led to mitigation of TDP-43 pathology, enhancement of autophagy, and amelioration of cognitive/motor deficits in CCH mice. Taken together, our results suggest that targeting TDP-43 pathogenic inclusions may have a disease-modifying effect in dementia caused by chronic brain hypoperfusion.

Key Words TDP-43 · Chronic cerebral hypoperfusion · Autophagy · NF-κb · Dementia

Introduction

Vascular dementia is the second most prevailing form of dementia in elderly population [1]. It is a progressive disease caused by a reduced blood flow going to the brain and eventually leading to a decline in cognitive abilities. In fact, certain regions of the brain that are responsible for memory, cognition, and behavior are particularly vulnerable to the loss of blood supply [2]. Chronic cerebral hypoperfusion (CCH) is one of the prime factors that contribute to development of vascular dementia in elderly patients. It can emerge from disorders that affect the cerebral circulating system like hypertension, diabetes, atherosclerosis, and smoking [3]. Furthermore, evidence suggests that chronic cerebral hypoperfusion causes neuronal damage in the cortex and hippocampal regions of the brain in various neurodegenerative diseases and cognitive disorders including Alzheimer's disease [4–7]. At present, the underlying molecular mechanisms by which cerebral vascular damage can induce cognitive deficits remain elusive [8]. In the past years, it has been suggested that chronic cerebral hypoperfusion may cause neurodegeneration through neuronal energy failure, by increasing the production of reactive oxygen species and proinflammatory cytokines by activated microglial cells that, in turn, damage the neuronal cells and confer lesions to the white matter in the cerebral cortex [9, 10].

✉ Jasna Kriz
jasna.kriz@fmed.ulaval.ca

1 CERVO Brain Research Centre, Quebec City, Canada

2 Research Centre of the CHU de Québec, Quebec City, Canada

3 Pathology Department of the CHU de Québec, Quebec City, Canada

4 Faculty of Pharmacy, Université Laval, Quebec City, Canada

5 Department of Psychiatry and Neuroscience, Facultyof Medicine, Université Laval, CERVO Brain Research Centre, 2601 Chemin de la Canardière, G1J2G3 Quebec City, Canada

Currently, one common and/or converging neuropathological pathway leading to dementia is the mislocalization and altered functionality of the trans-active response DNA binding protein 43 (TDP-43). TDP-43 belongs to the family of heterogeneous ribonuclear proteins highly conserved among species that regulate gene expression by controlling several RNA processes [11–13]. It is identified as a major constituent of ubiquitinated nuclear and cytoplasmic aggregates in several neurological disorders including frontotemporal lobar degeneration, ALS, and Alzheimer's disease [14–17].

Recently, we showed that neuronal damage following brain ischemia is characterized by an age-related increase and formation of ubiquitinated TDP-43 cytoplasmic inclusions in neurons and activated microglia [18]. The observed overexpression of cytoplasmic TDP-43 was associated with an age-dependent induction of the pathogenic NF-κB response that further exacerbated ischemic injury [18]. In keeping with our recent work, we hypothesized that a progressive ischemia-induced deregulation of TDP-43 represents a key molecular event in the pathogenesis of vascular dementia. To test it, we generated a mouse model (permanent occlusion of carotid artery in middle-aged mice) that mimics pathology associated with chronic cerebral hypoperfusion (CCH). Here, we report a marked increase in cytoplasmic TDP-43 in cortical neurons of CCH mice. The presence of the cytoplasmic TDP-43 immunoreactive structures was also detected in the post-mortem brain tissues from patients suffering from vascular dementia. The observed deregulation was associated with an altered inflammatory response and activation of pathogenic NF-κB pathways, as well as development of progressive cognitive and mild motor deficits. Treatment with a novel analog of withaferin A, an antagonist of NF-κB essential modulator (NEMO) [19–21], boosted autophagy and alleviated TDP-43 pathology and behavioral deficits in the CCH mice. These results suggest that NF-κB pathogenic signaling and autophagy may represent therapeutic targets in vascular dementia.

Methods

Animals

Wild-type (C57Bl/6) (WT) and toll-like receptor 2-luciferase-green fluorescent protein (TLR2-luc-GFP) male mice of 5–6 months old were selected for study. The TLR2-luc-GFP transgenic mice were developed and genotyped as described previously [22]. All mice were provided with water and healthy diet and monitored during the entire experimental protocol. All the experimental procedures were approved by the Laval University Animal care Ethics Committee and are in accordance with the *Guide to the Care and Use of Experimental Animals* of the Canadian Council on Animal Care. (Protocol # 17-133-1).

Surgical Procedure

Unilateral common carotid artery occlusion (UCCAO) was induced in 5-month-old male WT and TLR2-luc-GFP transgenic mice. Mice were anesthetized using 2% isoflurane in 100% oxygen at a flow rate of 1.5 L/min and kept on a heating pad to avoid fall in body temperature. The left common carotid artery (LCCA) was ligated using a non-absorbable 6-0 silk suture blocking permanently the CCA. The sham group of same age underwent similar procedure without ligating the LCCA. All the tissues from CTL and CCH group were collected for different biochemical analysis 8 weeks after surgery [23].

Administration of IMS-088

IMS-088, a withaferin A analog with a methyl at position $_4$–OH (acetylation), was kindly provided from IMSTAR therapeutics (Vancouver, Canada). IMS-088 was first dissolved in dimethyl sulfoxide and diluted in Tween 20 and 0.9% saline. The final concentration of dimethyl sulfoxide was 5% and tween 20 was 2.5%. The drug was prepared fresh every day. Male wild-type mice were divided randomly into two groups: (1) vehicle group which received vehicle (0.9% saline with 2.5% tween and 5% dimethyl sulfoxide) and (2) IMS-088 treatment group which received orally IMS-088 at 30 mg/kg body weight twice a day for 2 months. The treatment was initiated 72 h post-surgery.

In Vivo Bioluminescence Imaging

The images were obtained by using IVIS 200 imaging system (Perkin Elmer). Twenty minutes prior to imaging session, the mice were administered with D-luciferin (150 mg/kg) dissolved in 0.9% saline. The mice were then anesthetized in 2% isoflurane in 100% oxygen at a flow rate of 1.5 L/min, placed in a heated light-tight imaging chamber. All the animals were imaged before for baseline expression and then continued at 1 week, 3 weeks, 5 weeks, 7 weeks, and 8 weeks after UCCAO. Images were captured using a high sensitivity CCD camera with wavelengths ranging from 300 to 600 nm and exposure time for imaging of brain was set for 1 min. The bioluminescence emission was quantified by determining the total number of photons emitted per second (p/s) using live image 2.5 acquisition and imaging software. Region of interest measurements were used to convert surface radiance (p/s/cm^2/sr) to total flux of photons expressed

in photons/second. The data are represented as pseudocolor images indicating light intensity (red and yellow, most intense), which were superimposed over gray-scale reference photographs. Data are represented as fold change to baseline intensity [24].

Protein Lysate Preparation and Immunoblot Analysis

Cytoplasmic fraction was obtained as described earlier [25, 26]. A 500 mg of fresh brain tissue samples was transferred to 1 ml of cell lysis buffer (10 mM HEPES, 10 mM NaCl, 1 mM KH_2PO_4, 5 mM $MgCl_2$) and homogenized by applying two strokes in a glass homogenizer. Now, the suspension was incubated for 10 min on ice and then homogenized by applying six strokes in a motorized homogenizer at 250 rpm. Differential centrifugation was performed after restoration with 100 µl of 2.5 M sucrose. The first round of centrifugation was performed at 6300×*g* for 10 min at 4 °C. The supernatant collected from the first round of differential centrifugation was subjected for centrifugation at 14,000 rpm for 150 min and the supernatant collected was used as cytoplasmic fraction. Urea-sodium dodecyl sulfate (SDS) insoluble fraction was collected as described [27]. The protein levels from cytoplasmic and insoluble fraction were determined by Bradford method. Protein sample was separated by electrophoresis on polyacrylamide gel and transferred on to PVDF membrane. After blocking with 5% skimmed milk/5% BSA, the membranes were incubated overnight at 4 °C with primary antibodies against TDP-43 (Proteintech, 1: 5000), phospho-TDP-43 (Cosmo bio, 1:1000), Iba-1 (WAKO, 1:1000), phospho-p65 (cell signaling, 1:1000), p62 (Millipore, 1:1000), LC3b (Novus Bio, 1:5000), and Beclin (Novus Bio, 1:1000). After washes with phosphate buffer saline (PBS)-Tween-20 (0.1%), the membranes were incubated with respective secondary antibodies (1:5000) conjugated with peroxidase (Jackson laboratory, USA). The membranes were again washed in PBS-Tween and processed for development using chemiluminescent reagent (Thermo pierce, USA) and exposed for different time periods on care stream Biomax Light or MR film (Kodak, NY, USA) and results were analyzed using Image j software. The membranes were stripped and re-probed with anti-actin (Millipore, USA, 1:30,000) to determine equal loading of samples [28].

Tissue Collection and Immunohistochemistry

The mice were anesthetized and transcardially perfused with PBS 1× followed by 4% paraformaldehyde at pH 7.4. The brains were fixed overnight in 4% paraformaldehyde and then cryopreserved in 30% sucrose [28]. The fixed brains were sliced into 25 µm sections, washed with PBS, and blocked with 5% goat serum for 1 h. The sections were incubated overnight with respective primary antibodies (rabbit polyclonal TDP-43 (Proteintech, 1:1000), rabbit polyclonal phosphoTDP-43 (Cosmo bio, 1:500), rabbit polyclonal Iba1 (WAKO, 1:500), and rat monoclonal CD11b (Serotech, 1:500)) followed by incubation with respective fluorescent secondary antibodies (1:500) (Molecular probe).

Cytokine Array

The mouse cytokine array (Mouse Cytokine Antibody Array, Ray Biotech) was used to detect the levels of different cytokines in sham and chronic stroke operated mice. The array was performed according to the manufacturer's instructions. The protein lysates were obtained by homogenization of brains from respective groups using 1× cell lysis buffer (provided in the kit). The protein concentration was calculated for each sample and diluted to 300 µg in 1× blocking buffer. Samples for each group (3 mice/group) were pooled and incubated with array membrane overnight at 4 °C. After washes, the membranes were incubated with biotinylated antibody cocktail provided in the kit overnight at 4 °C, and next day following successive washes, membranes were incubated with 1× HRP-Streptavidin for 2 h at room temperature. The membranes were then processed according to Ray Biotech protocol. Membranes were exposed to Biomax Light or MR film (Kodak, NY, USA) and analyzed by ImageJ software.

Behavioral Tests

Passive Avoidance Test

Step through passive avoidance was performed as described previously [29] with few modifications and carried out in a box containing light and dark chambers separated by a small guillotine door. The test is carried for 3 days. On first day, mice are allowed to familiarize the box. On the second day, mice are placed in the light chamber, and when it enters the dark chamber, guillotine door was closed and a foot shock of 0.6 mA was given for 5 s. On the third day (test day), mice were placed in the light chamber and latency to enter the dark chamber was noted with a cut-off time of 300 s.

Novel Object Recognition Test

Novel object test was performed as described earlier [30, 31] with minor modifications. Test is performed for 3 days. On first day, mice are allowed to familiarize the box for 5 min. On the second day, the mice are

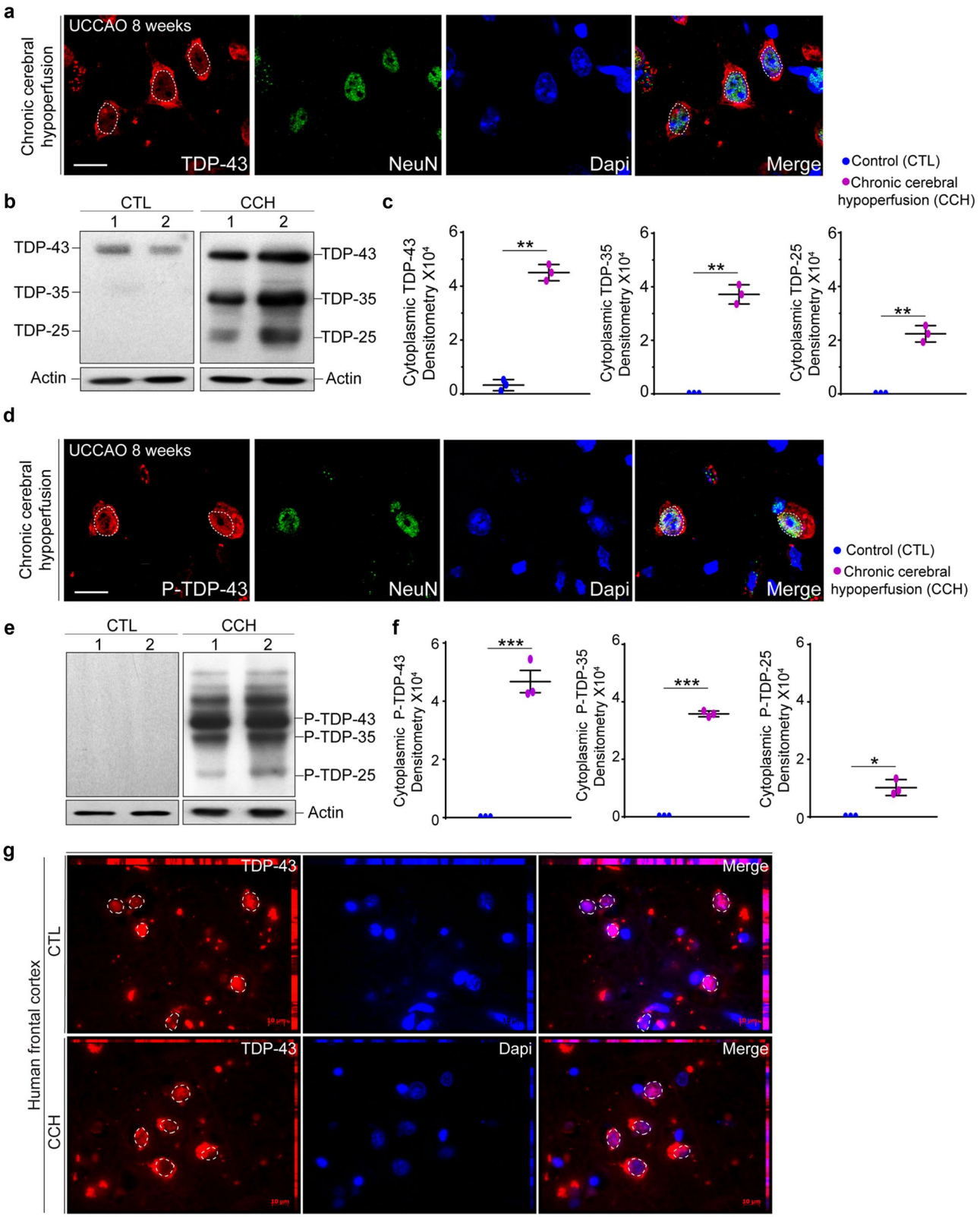

allowed to explore the two familiar objects for 5 min. On the third day (test day), one of the familiar objects is replaced with a novel object and a percent of time spent exploring the novel object relative to the total time spent exploring both objects can be a measure of novel object recognition.

◂**Fig. 1** TDP-43 pathology in mice subjected to chronic cerebral hypoperfusion (CCH) and in human vascular dementia. **a** Double immunofluorescence of the brain cortex sections of WT mice using TDP-43 antibody (red) and mouse monoclonal NeuN antibody (green) show mis-localization of TDP-43 in neuronal cells after 8 weeks of UCCAO. **b** Western blot of cytoplasmic lysates using TDP-43 antibody showed low levels of TDP-43 in control mice and a marked increase in TDP-43 after UCCAO. TDP-35 and TDP-25 expression are also found after CCH. **c** Normalized densitometry analysis reveals significant increase in the levels of whole length TDP-43, pathological TDP-35, and TDP-25 fragments in CCH mice compared with control. Actin is used as loading control. **d** Immunofluorescence using phospho-TDP-43 antibody (red) reveals neuronal cytoplasmic aggregates after CCH. **e** Western blot of urea-SDS insoluble fraction using phospho-TDP-43 in the control reveals no expression of phospho-TDP-43. On the opposite, CCH mice showed phospho-TDP-43, phospho-TDP-35, and phospho-TDP-25 expression. **f** Normalized densitometry analysis reveals significant increase in the levels of pathological phospho-TDP-35 and TDP-25 fragments, suggesting the formation of phospho aggregates after chronic cerebral hypo perfusion. **g** Representative photomicrographs of the human frontal cortex brain sections (3 patients and corresponding controls). Immunofluorescence analysis using TDP-43 antibody reveals cytoplasmic TDP-43 in cortical brain sections of the patient died from vascular dementia. Scale bar represents 10 µm. Entire data in the figure was presented as mean ± SEM and statistical significance between the groups was achieved using unpaired *t* test and depicted as $^{***}p<0.001$, $^{**}p<0.01$, $^{*}p<0.05$

Wire Hanging Test

Test was performed as described elsewhere with minimal modifications [32]. A wire of 55 cm length is stretched tightly between two stands and is maintained 35 cm above a layer of bedding material to prevent injury to the animal when it falls down. The animals are hanged with its fore limbs and time of fall is recorded. Test consists of three trials and average of three trails is recorded for analysis of motor activity.

Pole Test

Pole test is used to assess the motor impairment caused due to the cortical damage in the mice [33]. A vertical pole of 55 cm height and 1 cm wide is suspended above the ground level and mouse is placed at the top of the pole and time to descend is recorded. Test consists of three trials and average of three trails is recorded for assessing motor impairment.

Statistical Analysis

The data quantified was represented as mean ± SEM. Statistical analysis was carried using prism.7 (Graph Pad Software, La Jolla, CA, USA). Comparison between two groups was achieved by unpaired *t* test and comparisons between multiple groups were done using one-way ANOVA followed by Tukey's post hoc multiple comparison test. Statistical significance was defined when $^{****}P<0.0001$, $^{***}P<0.001$, $^{**}P<0.01$, $^{*}P<0.05$.

Human Subjects

The human post-mortem brain tissues were obtained from the archives of the pathology Department of the CHU de Québec. Brains were acquired under proper Institutional Review Board (IRB) protocols with informed consent for research from the subject or its family when deceased. The analysis of TDP-43 expression patterns was performed on frontal brain cortex sections of three patients and corresponding controls. They all presented with cerebrovascular disease confirmed by histological examination. The paraffin-embedded sections were subjected for immunofluorescence using human TDP-43 antibody and microscopic images were taken using Zeiss Apotome microscope. The human brain samples were collected after obtaining informed, written consent in accordance with the institutional human ethics committee guidelines.

Results

Chronic Cerebral Hypoperfusion Causes Deregulation of TDP-43 in Mouse and Human Disease

To date, the molecular mechanisms involved in the development of vascular dementia remain unclear. Recent evidence suggests that cerebrovascular pathology including stroke and chronic brain ischemia may cause deregulation of TDP-43 [29, 34]. Thus, we examined TDP-43 expression patterns in the model of chronic brain hypoperfusion that mimics cerebrovascular pathology in dementia. The analysis has been performed using the model of CCH caused by unilateral common carotid artery occlusion (UCCAO) in 5-month-old mice. As previously described by Qui and colleagues [35], hypoperfusion aggravated AD pathology in 3tg AD model starting 2 months after ligature. We first characterized the cellular expression patterns of TDP-43 8 weeks after UCCAO. The immunofluorescence analysis of the brain sections 2 months after CCH revealed a marked mislocalization of TDP-43 into cytoplasm of the cortical neurons (Fig. 1a). Under pathological conditions, TDP-43 can be cleaved to generate a 35 and 25 kDa C-terminal toxic fragments lacking the N-terminus nuclear localization signal [14, 36]. To further characterize expression profiles of mislocalized TDP-43, we collected the cytoplasmic fraction from the brain homogenates 8 weeks after UCCAO and age-matched controls. We observed a significant increase in the cytoplasmic whole length TDP-43 in the CCH mice when

compared with controls ($n=3$, $p<0.01$). The cytoplasmic cleaved fragments of TDP-35 ($n=3$, $p<0.01$) and TDP-25 ($n=3$, $p<0.01$) were also significantly increased in the cytoplasmic fraction from the brain homogenates from CCH mice and were not detectable in control samples (Fig. 1b, c). As reported earlier, these cleaved short fragments are more prone to modifications to generate insoluble pathological phosphorylated aggregates in the cytoplasm [37, 38]. To test this hypothesis, we searched for presence of phospho-TDP-43 aggregates in CTL and CCH brain sections. Double immunofluorescence analysis revealed the presence of punctuated phospho-TDP-43-positive aggregates in the cytoplasm of cortical neurons (Fig. 1d). In addition, Western blot analysis carried out on the insoluble protein fraction revealed a significant increase in the levels of phospho-TDP-43 ($n=3$, $p<0.001$), phospho-TDP-35 ($n=3$, $p<0.001$), and phospho-TDP-25 ($n=3$, $p<0.05$) aggregates in CCH mice thus further suggesting a possible pathogenic mechanism of TDP-43 deregulation (Fig. 1e, f). It is noteworthy that the cytoplasmic TDP-43-positive inclusions were almost exclusively present in neurons of the frontal cortex and to a lesser extent in hippocampus while other brain regions were devoid of mislocalized TDP-43. We recently showed that ischemic stroke in humans is associated with an increase in TDP-43 immunoreactivity in the cytoplasmic compartment. As the role of TDP-43 in the pathogenesis of vascular dementia remains elusive, we next asked whether similar deregulation of TDP-43 expression patterns occurs in the context of chronic brain hypoperfusion in human disease. Therefore, to further explore the role of TDP-43 in vascular dementia, we analyzed TDP-43 expression patterns in post-mortem human brain tissues. Representative micrographs revealed a presence of the cytoplasmic TDP-43 immunoreactive structures in the cortical neurons of patients suffering from vascular dementia. As further shown in Fig. 1g, the mislocalization of TDP-43 into cytoplasmic compartments of the affected neurons was associated with a partial nuclear exclusion of TDP-43 in the cortical neurons of patient suffering from vascular dementia when compared with controls suggesting a deregulation of TDP-43 in human disease.

Live Imaging of Innate Immune Response Reveals Chronic Microgliosis in CCH Mice

It has been widely established that in neurodegenerative diseases, such as ALS and/or FTLD, mislocalization of TDP-43 is also present in non-neuronal cells including astrocytes and microglia [39]. In the current study, double immunofluorescence analysis of the CCH brain sections revealed deregulation of TDP-43 in microglial cells, as revealed by a marked co-localization of TDP-43 with a microglial marker Iba1. In fact, we observed a marked deregulation of TDP-43 in activated microglia as it was detected in the cytoplasm of the Iba1-positive cells (Fig. 2a). The observed deregulation of TDP-43 in microglial cells was predominant in the frontal cortex. To further characterize dynamics of microglial activation following UCCAO, we took advantage of the TLR2-luc-GFP mice previously generated in our laboratory [22]. In these mice, activation of microglial cells and/or induction of TLR2 signaling can be captured from the brains of living mice by bioluminescence/biophotonic imaging. In our experimental protocol, the mice were imaged over the time period of 8 weeks following initial surgery (UCCAO). As shown in Fig. 2 b and c, we observed a 2.5-fold increase in TLR2 induction 1 week after UCCAO when compared with baseline values. The TLR2 intensity dropped slightly in the 3rd week but it remained significantly increased over 8 weeks. The 3D reconstruction of the TLR2 signal 1 week after UCCAO revealed the highest TLR2 signal/microglial activation intensity in olfactory bulb and more distal regions of the brain including parts of the cortex and hippocampus (Fig. 2d). The findings from in vivo imaging experiments were further confirmed by immunofluorescence and Western blot analyses using Iba-1 and TLR2 antibodies. As shown in Fig. 2e, microglial cells after 8 weeks of CCH displayed bigger soma and less ramifications suggesting morphologically more activated phenotypes while Western blot analysis from the cortical brain tissue homogenates revealed a significant increase in the expression levels of TLR2 ($n=3$, $p<0.05$) and Iba1 ($n=3$, $p<0.01$) 8 weeks after CCH (Fig. 2f, g).

Chronic Hypoperfusion Increases NF-κB-Mediated Neuroinflammation and Neuronal Death

We recently showed that deregulation in TDP-43 following acute brain ischemia induces age-dependent induction of pathogenic NF κB signaling acting as co-activator or inhibitor of the p65 subunit of NF-κB [18]. In the current project, we analyzed the levels of phospho-P65 by performing Western blots on the nuclear fraction of cortical lysates of CTL and CCH mice. The densitometry analysis showed a significant increase in the level of nuclear phosphor-P65 ($n=3$, $p<0.05$) in the CCH mice, suggesting that mislocalization and formation of insoluble phospho-TDP-43 aggregates trigger NF-κB inflammatory pathway in these mice (Fig. 3a). As NF-κB modulator, TDP-43 may also regulate the levels of inflammatory cytokines and control the neuronal death [39]. As expected, the activation of NF-κB pathway resulted in production of pro-inflammatory cytokines. In fact, in our CCH group, we found significant increase in the levels of proinflammatory cytokines like IL-1β ($n=3$, $p<0.001$), IL-6 ($n=3$, $p<0.01$), IL-17 ($n=3$, $p<0.05$), and TNF-α ($n=3$, $p<0.001$) when compared with the CTL group

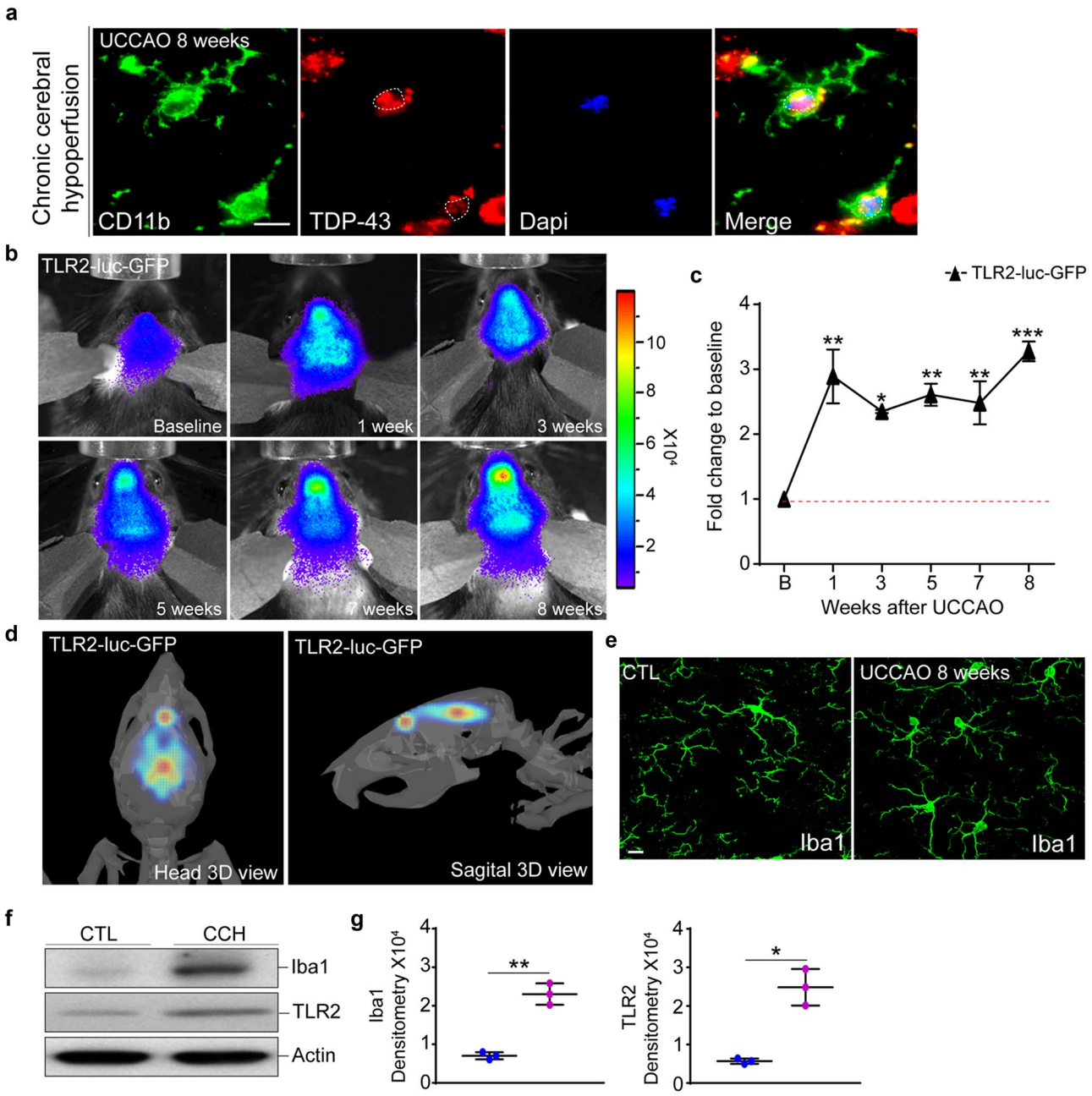

Fig. 2 Mislocalization of TDP-43 in activated microglia after chronic cerebral hypoperfusion. **a** Double immunofluorescence of the brain cortex sections using TDP-43 antibody (red) and CD11b antibody (green) show mislocalization of TDP-43 in microglial cells after CCH in WT mice. **b** Real-time bioluminescence imaging of microglial activation in TLR2-luc-GFP mice weeks after UCCAO. The color calibrations at the right are photon counts. **c** Data plotted was obtained measuring the photon emission. Black line shows the induction of TLR2 signals. After 1 week, the TLR2 signals increased and remain constant 8 weeks after surgery. **d** 3D reconstruction of TLR2 expression. Top of the head and sagittal view of the reconstructed bioluminescent signal 1 week after UCCAO. **e** Immunofluorescence analysis using microglial marker Iba1 reveals activated microglial cells after CCH when compared with control mice. **f** Western blot analysis of cortical lysates from the control and CCH mice using rabbit polyclonal iba-1 and rabbit polyclonal TLR2 shows expression of iba-1 and TLR2. **g** Normalized densitometry analysis revealed a significant increase in the levels of Iba1 and TLR2 after chronic cerebral hypo perfusion. Scale bar represents 10 µm. Entire data in the figure was presented as mean ± SEM and statistical significance between the groups was achieved using unpaired *t* test and depicted as $^{***}p<0.001$, $^{**}p<0.01$, $^{*}p<0.05$

(Fig. 3b). Interestingly, the levels of two anti-inflammatory cytokines IL-4 and IL-10 were also significantly increased in the CCH when compared with control ($n=3$, $p<0.001$). We also analyzed monocyte/macrophage colony growth factors such as MCSF, GM-CSF, and GSCF. As shown in Fig. 3b, levels of MCSF and GM-CSF were significantly increased ($n=3$, $p<0.01$ and $p<0.001$) while no significant change has been observed in the levels of GSCF. As further shown in Fig. 3c, Western blot analysis revealed an increase in expression levels of apoptotic marker cleaved caspase-3, in CCH mice compared with CTL mice. Hence, activation of NF-κB signaling and associated alteration in brain cytokine/chemokine profiles are associated with increased cellular death 8 weeks after UCCAO ($n=3$, $p<0.05$).

UCCAO Induces Cognitive Deficits and Motor Impairments in Middle-Aged Mice

It has been suggested that CCH may represent a key pathogenic mechanism leading to vascular cognitive impairment and ultimately to dementia [40]. Mimicking the CCH, the unilateral common carotid artery occlusion drops the blood supply to subcortical regions of the brain, induces hypoxia, and causes neuronal damage leading to anxiety, dementia, and motor deficits in long term [41, 42]. In order to assess the effects of UCCAO on development of cognitive impairment, in the current study, we used passive avoidance and novel object recognition test. As in previous experiments, behavioral analyses were performed 8 weeks after UCCAO. Remarkably, in our experiments, we found that the percentage of the time spent exploring the novel object was significantly decreased ($n=9$ mice, $p<0.001$) at 8 weeks after UCCAO in comparison with the respective controls (Fig. 3d). Passive avoidance paradigm was employed to further confirm cognitive deficits. The latency to enter the dark chamber of the testing box was significantly decreased ($n=7$, $p<0.01$) in CCH mice in comparison with the respective CTL mice (Fig. 3e). Motor performance in mice 2 months after UCCAO was assessed by the wire hang test. As shown in Fig. 3e, the average latency of time to fall was less ($n=9$, $p<0.001$) in the CCH mice in comparison with the respective control mice. Indeed, the CCH mice did not hang on the wire for a long time suggesting a significant decrease in motor performance in these mice (Fig. 3f). Pole test was also performed after CCH, and in accordance with our previous results, we found that the time taken to descend the pole by CCH mice was significantly increased ($n=9$, $p<0.01$) compared with control mice further confirming existence of motor impairments at 8 weeks after UCCAO (Fig. 3g). Taken together, our results strongly suggest that once initiated in middle-aged mice, a CCH leads to marked cognitive impairments and motor deficits. The main neuropathological features associated with the observed cognitive and motor deficits were a robust TDP-43 proteinopathy and neuroinflammation.

IMS-088 Restores the Nuclear TDP-43 and Alleviates the Formation of TDP-35 and TDP-25 Pathological Fragments

The therapeutic potential of herbal medicine *Withania somnifera* (or Ashwagandha) and of its active product withaferin A, a known inhibitor of NF-κB signaling, have been demonstrated in a mouse model of FTD as well as in different models of ALS [29, 43, 44]. The therapeutic effects of natural products such as Ashwagandha are difficult to evaluate due to questionable stability of natural products and variability in the concentration of active components. Withaferin A, a steroid lactone, is a major active component of Ashwagandha known to be an inhibitor of NF-κB signaling via antagonizing the function of NF-κB essential modulator (NEMO) [20, 21]. Here, we have tested a semi-synthetic analog of withaferin A called IMS-088 which has a methyl group at position $_4$–OH (acetylation). IMS-088 compound was kindly provided from Imstar therapeutics (Vancouver, Canada).

According to a protocol established by Imstar therapeutics, the IMS-088 (30 mg/kg) was delivered orally (by gavage) twice a day starting 72 h after initial UCCAO. Immunofluorescence analysis was performed on the brain sections of both IMS-088- and vehicle-treated group. As expected, TDP-43 was detected in the nucleus of cortical cells in the CTL group (Fig. 4a) whereas we observed a marked mislocalization of TDP-43 into the cytoplasm with a strong exclusion of TDP-43 from the nucleus in the vehicle-treated group with CCH (Fig. 4b). Remarkably, the CCH mice treated with IMS-088 for 8 weeks exhibited a strong nuclear TDP-43 staining in the cortical neurons whereas few cells exhibited diffused cytoplasmic TDP-43 (Fig. 4c). Nuclear vs cytoplasmic expression patterns of TDP-43 were further confirmed by Western blots performed on the nuclear and the cytoplasmic lysates collected from the control and CCH mice treated with vehicle or IMS-088. As shown in Fig. 4 d and e, we observed a significant reduction in the cytoplasmic TDP-43 levels after IMS-088 treatment when compared with the vehicle group ($n=3$, $P<0.001$). There was also reduction of TDP-35 ($n=3$, $P<0.01$) and TDP-25 ($n=3$, $P<0.001$) pathological fragments in the CCH mice after treatment with IMS-088 in comparison with vehicle-treated group. The expression of nuclear TDP-43 (Fig. 4f, g) was significantly increased with IMS-088 treatment ($n=3$, $P<0.01$) when compared with vehicle group suggesting that IMS-088 treatment restored the nuclear expression of TDP-43 in the CCH model.

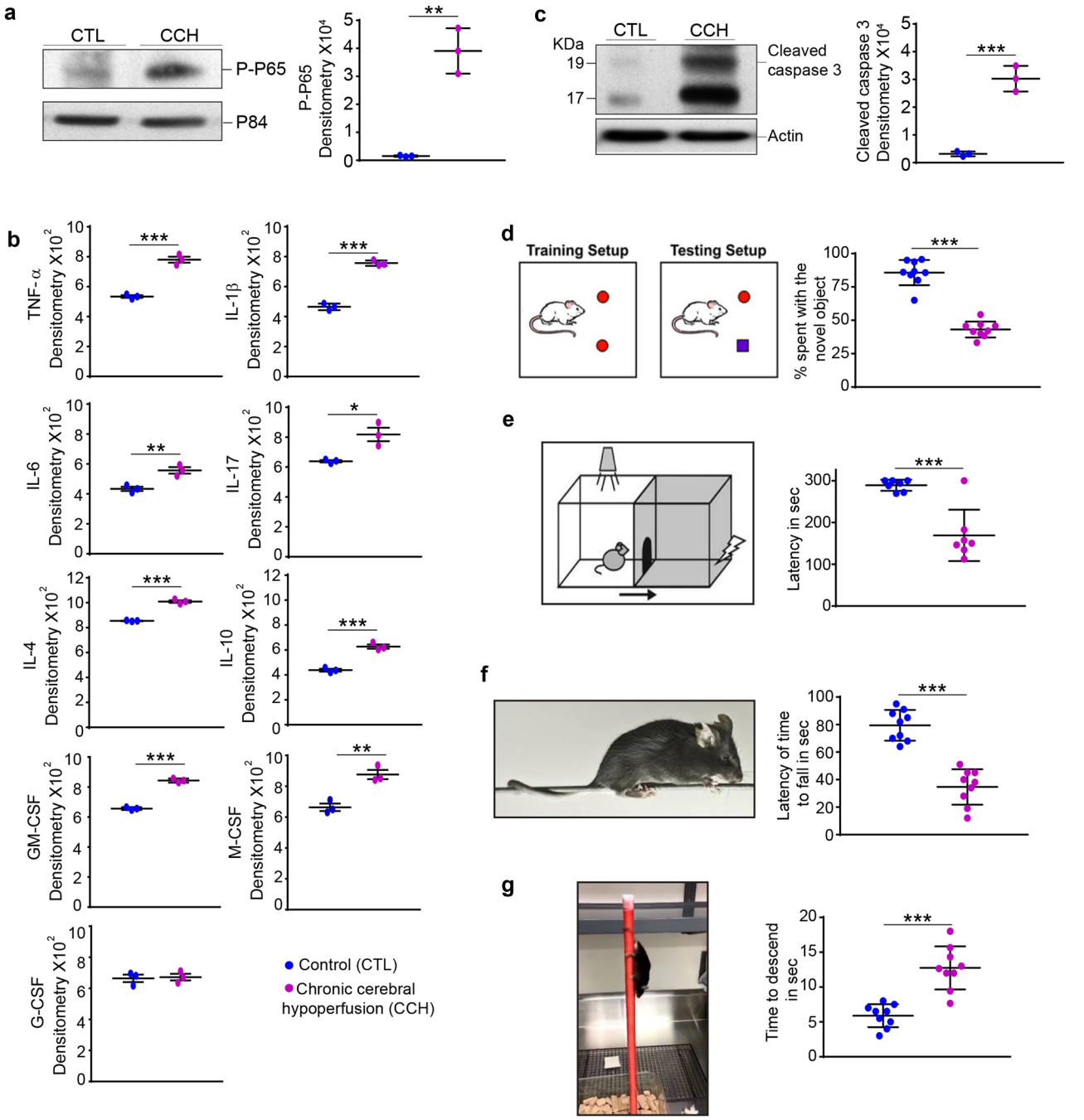

Fig. 3 CCH causes activation of NF-κB, cell death, cognitive decline, and motor impairment. **a** Western blot of nuclear lysates using phospho-P65 shows a significant increase in the levels of phospho-P65 after CCH when compared with control mice. P84 is used as loading control. **b** Levels of pro-inflammatory and anti-inflammatory cytokines and growth factors were significantly increased after CCH. **c** Western blot and densitometric analysis of cortical lysates using cleaved caspase-3 show a significant increase in the levels of cleaved caspase-3 after CCH. **d** Novel object recognition test showing the % time spent with novel object by control and CCH mice. **e** Passive avoidance test showing latency to enter the dark chamber by control and CCH operated mice. **f** Wire hang test showing the latency of time fall from the wire by control and CCH-operated mice. **g** Pole descend test showing time of descend by control and CCH mice. Entire data in the figure was presented as mean ± SEM and statistical significance between the groups was achieved using unpaired *t* test and depicted as $^{***}p<0.001$, $^{**}p<0.01$, $^{*}p<0.05$

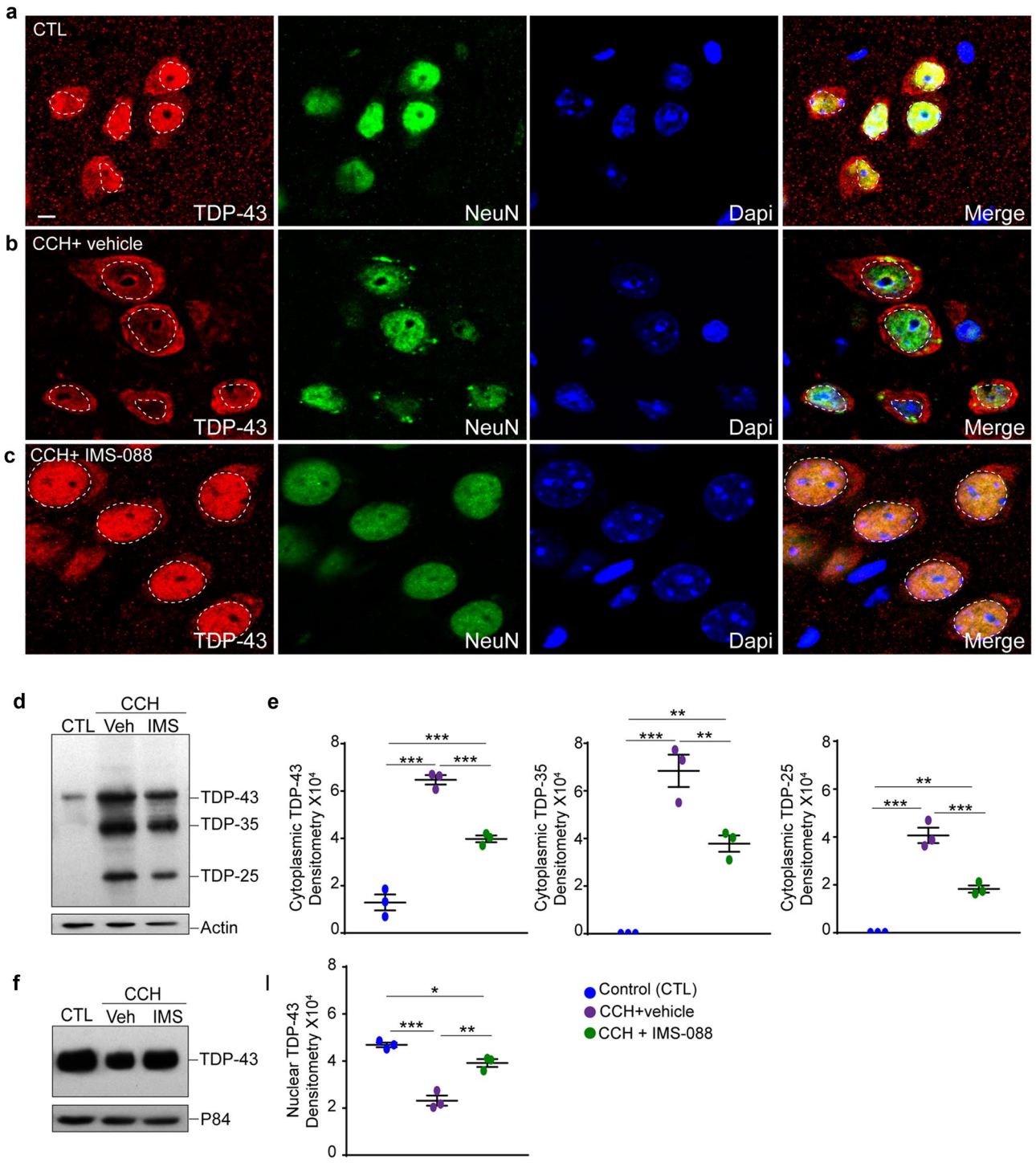

Fig. 4 IMS-088 restores TDP-43 mislocalization and reduces formation of TDP-35 and TDP-25 fragments. **a–c** Double immunofluorescence of the cortical brain sections using TDP-43 (red) and NeuN antibody (green) shows that TDP-43 is localized in the nucleus of the neurons in control and CCH mice treated with IMS-088, whereas in CCH mice treated with vehicle TDP-43 is mislocalized into cytoplasm. **d** Western blot of cytoplasmic lysate collected from the control, CCH mice treated with vehicle or IMS-088 using TDP-43 reveals the different expression of TDP-43 and fragmented pathological TDP-35/25 in all groups. **e** Normalized densitometry analysis reveals a significant decrease in the expression levels of whole length TDP-43 and pathological fragmented TDP-35/TDP-25 levels in the CCH mice treated with IMS-088 in comparison with vehicle-treated group. **f** Western blot of nuclear lysate collected from the control, CCH mice treated with vehicle or IMS-088 using TDP-43 reveals the different level of expression of TDP-43. **g** Normalized densitometry analysis shows significant increase in the expression of whole length TDP-43 in CCH mice treated with IMS-088 in comparison with vehicle-treated group. Entire data in the figure was presented as mean ± SEM and statistical significance between the groups was achieved using ANOVA followed by Tukey's multiple comparison test and depicted as $^{***}p < 0.001$, $^{**}p < 0.01$, $^{*}p < 0.05$

Decreased Microglial Activation in IMS-088-Treated Mice

IMS-088 acts as regulator of immune response by reducing inflammation via the NF-κB pathway. Here, we analyzed the effect of IMS-088 on microglial activation in CCH mice. As shown in Fig. 5a, we observed fewer microglial cells in control mice and IMS-088-treated mice when compared with vehicle-treated group suggesting that IMS-088 is able to reduce the microglial activation induced by CCH. At higher magnification (Fig. 5b), microglial cells from controls showed extended ramification suggesting a resting state whereas microglia from the vehicle-treated CCH mice showed shorter ramifications and a bigger soma, an indication for reactive state, whereas in the IMS-088-treated CCH, the morphological phenotypes of microglia were more resting-like cells. As shown in Fig. 5c, the quantification of Iba1-positive microglial cells per unit square area from control mice and CCH mice treated with vehicle or IMS-088 revealed a significant increase in the number of Iba1-positive cells in the cortex of CCH mice treated with vehicle ($n=3$, $P<0.001$) when compared with control mice. In contrast, treatment with IMS-088 ($n=3$, $P<0.0001$) significantly reduced the number of Iba1-positive cells in CCH mice in comparison with CCH mice treated with vehicle. To further confirm the reduction in the numbers of microglial cells, we collected the cortical lysates from the control, CCH mice

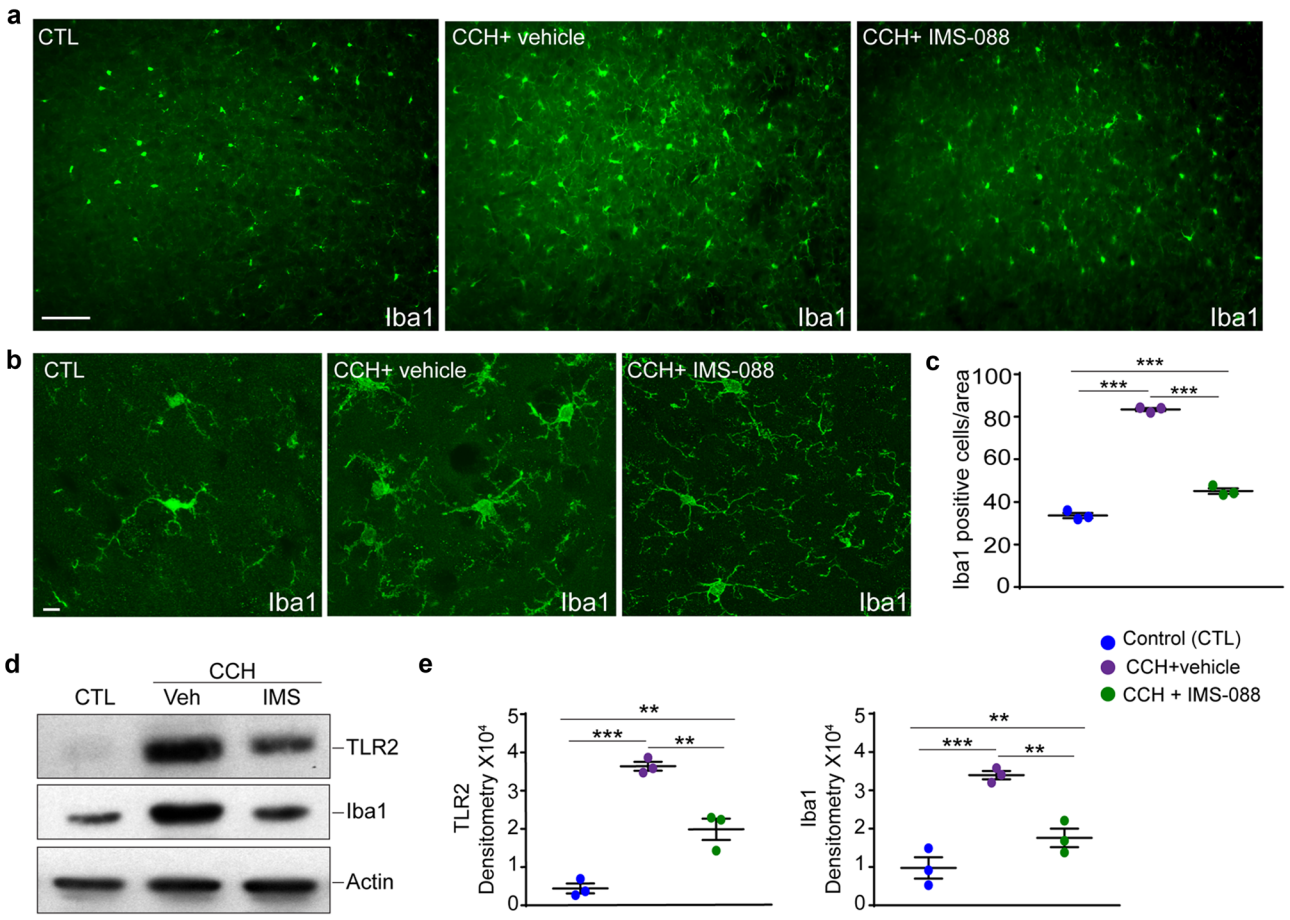

Fig. 5 IMS-088 attenuated microgliosis after CCH. **a** Immunofluorescence analysis of Iba1 immunostaining in cortical sections from the control and CCH mice treated with vehicle or IMS-088. **b** Confocal images of Iba1 staining showing difference in the morphology of microglial cells in control (small soma-longer ramifications), CCH mice treated with vehicle (larger soma and short ramifications), and IMS-088 (small soma and longer ramifications). **c** Number of Iba1-positive cells per unit square area from control and CCH mice treated with vehicle or IMS-088 group were counted using Image J software**.** Significant reduction in the number of microglial cells per unit area is found in the CCH mice treated with IMS-088 in comparison with vehicle-treated group. **d** Western blot of whole cortical lysate using TLR2 and Iba1 antibodies shows the different levels of Iba1 and TLR2 expression in all 3 groups. **e** Normalized densitometry analysis shows a significant decrease in the levels of TLR2 and Iba1 in the CCH mice treated with IMS-088 in comparison with vehicle group. Scale bar represents 10 and 50 µm. Entire data in the figure was presented as mean ± SEM and statistical significance between the groups was achieved using ANOVA followed by Tukey's multiple comparison test and depicted as $^{***}p<0.001$, $^{**}p<0.01$

treated with vehicle or IMS-088, and analysed the expression levels of Iba1 and TLR2 proteins by Western blot. The normalized densitometry analysis revealed a significant increase in the levels of TLR2 and Iba1 in the CCH mice compared with controls (Fig. 5e, TLR2: $n=3$, $P<0.001$; Iba-1: $n=3$, $P<0.001$). Supporting the immunofluorescence data, the levels of TLR2 and Iba1 were significantly reduced in the cortex of IMS-088-treated mice (Fig. 5e, TLR2: $n=3$, $P<0.01$; Iba-1: $n=3$, $P<0.01$). Both the immunofluorescence and the Western blot analyses clearly demonstrated that IMS-088 moderated the inflammatory response following CCH.

Inhibition of NF-κB Ameliorates Cognitive and Motor Performance in CCH Mice

Next, we examined whether IMS-088-mediated regulation of NF-κB signaling had an effect on cognitive and motor symptoms after CCH. The cognitive behavior of the CCH mice was assessed using passive avoidance test following 8 weeks of treatment with IMS-088. Remarkably, latency to enter the dark compartment by the IMS-088-treated CCH mice was significantly increased ($n=13$, $P<0.001$) compared with the vehicle-treated group to reach control levels as previously shown (Fig. 6a), suggesting a significant therapeutic effect of IMS-088 on cognitive performance. The effects of IMS-088 were also tested in the novel object discrimination test. The percentage of the time spent with the novel object was significantly increased in the CCH mice treated with IMS-088 ($n=13$, $P<0.001$) when compared with the vehicle-treated group (Fig. 6b). The results obtained in these two cognitive tests suggest that 8 weeks of IMS-088 treatment significantly improved cognition and memory in CCH mice model. To assess the effects of IMS-088 treatment on motor balance and coordination, we performed the four limb grid hanging test. The CCH mice treated with IMS-088 ($n=13$, $^{***}P<0.001$) for 8 weeks exhibited a significant increase in the time before falling when compared with the CCH mice treated with vehicle (Fig. 6c). To further confirm the therapeutic effects of IMS-088 on motor balance, we used the forelimb wire hanging test. Once again, the CCH mice treated with IMS-088 ($n=13$, $P<0.001$) showed a significant increase in the time before falling from the wire in comparison with CCH mice treated with vehicle (Fig. 6d). Finally, as shown in Fig. 6e, pole descend test was used to confirm the effects of IMS-088 on motor coordination. Importantly, the IMS-088-treated mice ($n=13$, $P<0.001$) were quicker to descend the pole than the vehicle-treated group. Hence, our results clearly suggest that treatment with IMS-088 improved cognitive impairments and motor deficits caused by CCH.

IMS-088 Promotes Clearance of the Insoluble Phospho-TDP-43 Aggregates by Enhancing Autophagy

While the role of IMS-088 in suppressing inflammation is in line with its expected inhibition of the NF-κB signaling, the effects of IMS-088 on the formation of phosho-TDP-43 aggregates suggest some additional therapeutic properties. As shown in Fig. 7a, we observed a significant reduction in the whole length phospho-TDP-43 and pathological phospho-TDP-35 and phosp-TDP-25 following IMS-088 treatment. In fact, normalized densitometry analysis(Fig. 7b) confirmed a significant decrease in the formation of phospho-TDP-35 and phosp-TDP-25 fragmented aggregates in the IMS-088-treated mice in comparison with CCH mice treated with vehicle (phospho-TDP-43: $n=3$, $P<0.05$; phospho-TDP-35: $n=3$, $P<0.05$; phospho-TDP-25: $n=3$, $P<0.001$). To address the mechanism of clearance/reduction of insoluble phospho-TDP-43 aggregates in IMS-088-treated mice, we examined the levels of autophagy markers like LC3B, beclin, and p62 using Fig. 7c. Normalized densitometry analysis revealed a significant increase in the levels of beclin ($n=3$, $P<0.05$), LC3BI ($n=3$, $P<0.05$), and LC3BII ($n=3$, $P<0.001$) when compared with vehicle-treated CCH mice with the level of LC3B II and beclin reaching the control level (Fig. 7d). We observed a significant decrease in the P62 levels ($n=3$, $P<0.05$) in the IMS-088-treated CCH mice in comparison with the vehicle-treated controls. Together, our results revealed that IMS-088 treatment promoted autophagy thus helping clearance of the insoluble TDP-43 aggregates. Importantly, the level of P62 was restored to the control levels in CCH mice treated with IMS-088 treatment (Fig. 7d). Next, to confirm and to validate the impact of IMS-088 on NF-κB inhibition, we measured the levels of nuclear phospho-p65. As shown in Fig. 7e, we found a significant reduction in the phospho-p65 levels after IMS-088 treatment ($n=3$, $P<0.05$) in comparison with the CCH mice treated with vehicle.

Finally, in order to determine if the treatment with IMS-088 had an effect on cell survival after CCH, we collected the cytoplasmic lysates from the control and CCH mice treated with vehicle and IMS-088 and examined the expression levels of apoptotic marker, cleaved caspase 3, (Fig. 7g). Normalized densitometry revealed a significant decrease in the CCH mice treated with IMS-088 ($n=3$, $P<0.05$) in comparison with vehicle-treated CCH mice demonstrating that IMS-088 improved cell survival after

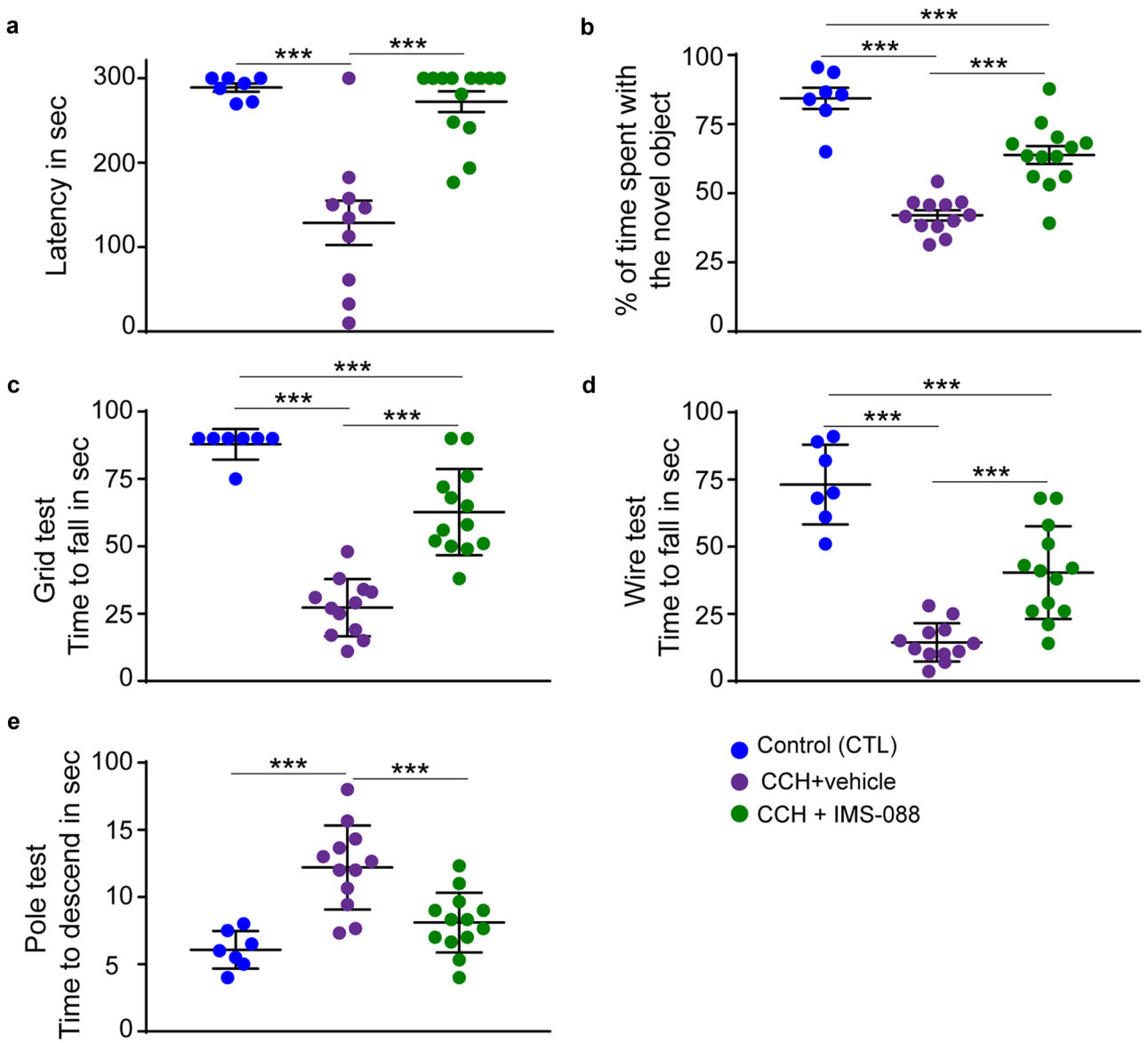

Fig. 6 IMS-088 improves cognitive and motor performance in CCH mice. **a** Passive avoidance test showing latency to enter the dark compartment in control, CCH mice treated with vehicle or IMS-088. Latency to enter the dark compartment was significantly increased in CCH mice treated with IMS-088 in comparison with vehicle-treated group. **b** Novel recognition test showing percentage time spent with novel object in control, CCH mice treated with vehicle or IMS-088. Percentage of the time spent with novel object was significantly increased in CCH mice treated with IMS-088 in comparison with vehicle-treated group. **c** Grid test showing the time of fall from the grid in control, CCH mice treated with vehicle and IMS-088. Time of fall from the grid was significantly increased in the CCH mice treated with IMS-088 in comparison with vehicle group. **d** Wire hang test showing time of fall from the wire in control, CCH mice treated with vehicle and IMS-088. Time of fall was significantly increased in the CCH mice treated with IMS-088 in comparison with vehicle group. **e** Pole test showing a time to descend in the control, CCH mice treated with vehicle and IMS-088. Time to descend pole was significantly decreased in CCH mice treated with IMS-088 in comparison with vehicle group. Entire data in the figure was presented as mean ± SEM and statistical significance between the groups was achieved using ANOVA followed by Tukey's multiple comparison test and depicted as $^{***}p < 0.001$

chronic cerebral hypoperfusion (Fig. 7h). Taken together, our results suggest that, in the context of disease caused by CCH, IMS-088 acts as inhibitor of the pathogenic NF-κB signaling and enhancer of autophagy thereby protecting ischemia-affected neurons against TDP-43-mediated pathology.

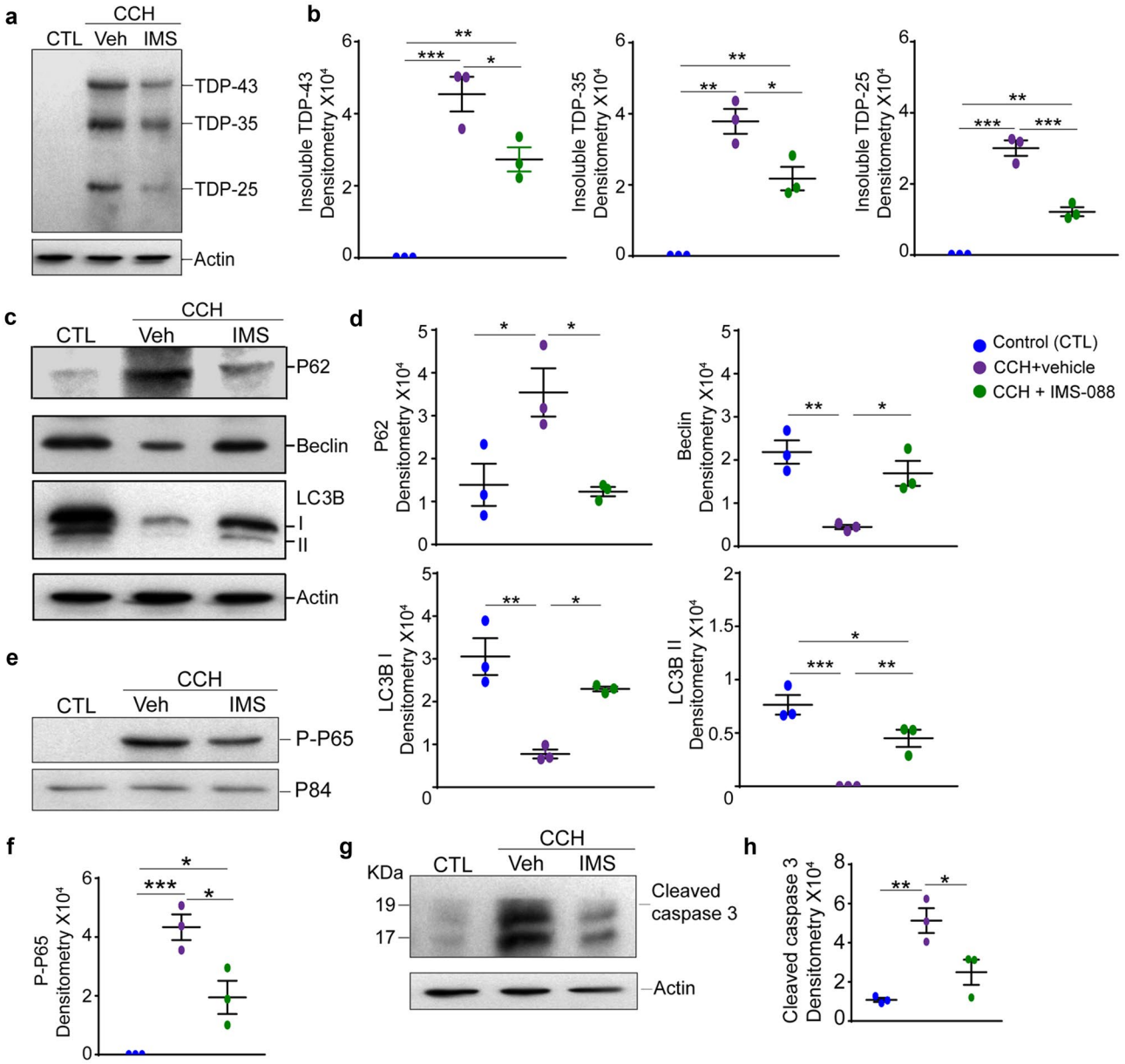

Fig. 7 IMS-088 enhances autophagy and clearance of cytoplasmic TDP-43 aggregates and reduced NF-κB activation and apoptosis. **a** Western blot of urea-SDS insoluble fraction using anti-phospho-TDP-43 antibody in both vehicle- and IMS-088-treated CCH mice. **b** Normalized densitometry analysis reveals a significant decrease in levels of phospho-TDP-43 and pathological fragmented phospho-TDP-35/25 aggregates in CCH mice treated with IMS-088 in comparison with vehicle-treated group. **c** Western blot of cortical lysates using autophagy markers p62, beclin, and LC3BI and LC3BII in control and CCH mice treated with vehicle or IMS-088. **d** Normalized densitometry analysis shows significant reduction in p62 levels, and significant increase in the levels of beclin, LC3BI, LC3BII in the CCH mice treated with IMS-088 in comparison with vehicle-treated group suggesting autophagy clearance of aggregated proteins was promoted by IMS-088. **e** Western blot of nuclear lysates using phospho-p65 in the control and CCH mice treated with vehicle or IMS-088. **f** Normalized densitometry analysis shows significant reduction in the levels of phospho-p65 in the CCH mice treated with IMS-088 in comparison with vehicle-treated group. **g** Western blot of cytoplasmic lysates using cleaved caspase-3 in the control and CCH mice treated with vehicle or IMS-088. **h** Normalized densitometry shows significant reduction in the levels cleaved caspases-3 in the CCH mice treated with IMS-088 in comparison with vehicle-treated group. Entire data in the figure was presented as mean ± SEM and statistical significance between the groups was achieved using ANOVA followed by Tukey's multiple comparison test and depicted as $^{***}p < 0.001$, $^{**}p < 0.01$, $^{*}p < 0.05$

Discussion

While a role for TDP-43 in the pathogenesis of frontotemporal dementia has been widely established [45], the work presented here provides compelling evidence for TDP-43 involvement in vascular dementia. Furthermore, the results strongly suggest that targeting autophagy and TDP-43 pathogenic inclusions may have a disease-modifying effect in dementia caused by chronic brain hypoperfusion. Here, we report that (1) CCH induced cytoplasmic mislocalization of TDP-43 and formation of insoluble phospho-TDP-43 aggregates as well as cleaved TDP-35 and 25 toxic fragments in cortical neurons; (2) CCH is associated with a deregulation of TDP-43, early activation of microglial cells, and NF-κB immune signaling as well as development of cognitive and motor deficits; (3) treatment of CCH mice with an analog of withaferin A which is a NEMO antagonist restored the balance between the nuclear *vs* cytoplasmic TDP-43 and alleviated behavioral deficits; and (4) IMS-088 acted as inducer of autophagy.

Vascular dementia is one of the most common causes of dementia in aging population, and to date, there is no certified treatment for this disease [46]. In spite of research efforts, understanding of the molecular mechanisms involved in the development of disease and the correlation between the cerebrovascular pathology and the cognitive impairments and/or dementia remain unclear. Here, the characterization of mice subjected to UCCAO surgery revealed that chronic brain hypoperfusion causes severe TDP-43 pathology in cortical neurons, a phenomenon which was also detected in post-mortem brain samples of patients who suffered from vascular dementia (Fig. 1g). TDP-43 is normally localized in the nucleus. The cytoplasmic TDP-43 aggregates, observed in pathological conditions, are associated with depletion of TDP-43 nuclear protein and a loss of its normal function [47]. In the CCH mouse model, we observed cytoplasmic mislocalization of TDP43, formation of highly phosphorylated TDP-43 aggregates, and increased levels of its pathogenic fragments such as phospho-TDP25 and phospho-TDP35. The TDP-43 pathology in the CCH mice is reminiscent of TDP-43 abnormalities found in FTD and ALS [15]. In the CCH mouse model of vascular dementia, the TDP-43 pathology was associated with an increase in apoptotic neuronal cell death, microglial activation, and increased levels of pro-inflammatory cytokines. Furthermore, the nuclear p65 NF-κB levels were increased reflecting abnormal activation of NF-κB signaling. Notably, the TDP-43 pathology in CCH mice was associated with development of marked cognitive and motor impairment.

NF-κB has been shown to have pivotal role and acts mediator of inflammatory cascades in TDP-43-mediated pathology [29, 48]. TDP-43 overexpression in BV2 cells caused elevated inflammatory responses to LPS while TDP-43 small interfering RNA (siRNA) reduced the activation of NF-κB in those cells [48]. Furthermore, mutant or truncated form of TDP-43 can directly activate microglial cells via NF-κB and the NLRP3 inflammasome triggering proinflammatory signals promoting motor neuron injury [49]. In human subjects with ALS or mild cognitive impairment, it was also reported that TDP-43 can interact with the P65 subunit of NF-κB [50]. Neuron-specific inhibition of NF-κB signaling was found to mitigate TDP-43 neuropathology [51].

IMS-088 is a novel semi-synthetic analog of withaferin A, a compound extracted from the medicinal plant *Withania somnifera* which is an inhibitor of NF-κB activity. Many reports described the effect of withaferin A on suppression of NF-κB activation, but the mechanism has only been unraveled recently. At first, this compound was described as an inhibitor of IκB kinase (IKKβ) [52] but subsequent studies rather suggested that withaferin A was a weak direct IKKβ inhibitor and that it inhibited IKK function by binding and disrupting NEMO reorganization into ubiquitin-based signaling structures [19–21]. Our group reported previously that inhibition of NF-κB signaling by withaferin A conferred protection mouse models of ALS [44, 48]. This has been further supported by a more recent work revealing that treatment with withaferin A alleviates TDP-43 pathology and cognitive impairment in a mouse model of FTDL [53]. IMS-088 is a semi-synthetic analog of withaferin A with improved tolerability and satisfactory blood-brain barrier penetration. The IMS-088 compound is basically the 4-O-methyl withaferin-A. Here, our results provide evidence of effective therapeutic effects of IMS-088 administered orally twice a day (30 mg/kg) in mice subjected to brain hypoperfusion by mitigating TDP-43 pathology and alleviating the cognitive/motor deficits. Furthermore, IMS-088 decreased NF-κB activation and reduced neuroinflammation.

It is noteworthy that IMS-088 treatment led to induction of autophagy. Autophagy is constitutively active in neurons and plays a significant role in cellular homeostasis by clearing the dysfunctional organelles and abnormal protein. When a cell is stressed during an injury or energy deprivation, it results in endoplasmic reticulum stress and involves impaired synthesis and mis-folding of the protein [54]. In most of the neurodegenerative disease, like in ischemic and hypoxic injury of the brain, the unfolded/misfolded protein response in the endoplasmic reticulum initiates autophagy to correct the protein misfolding and persistent stress affecting the cellular function, neurotransmission impairment, and neuronal death [55–58]. It has been reported that autophagy impairment by mammalian TOR activation causes abnormal accumulation of tau in

Alzheimer's disease mice subjected for CCH [35]. Another study reported that Arginine vasopressin, endogenous non-peptide hormone reverses the spatial learning memory impairments in a CCH rat model by promoting autophagy signaling partially [59]. In vitro studies on different cancer cell lines revealed that TNF-dependent NF-κB activation represses autophagy and that withaferin A can promote autophagy [60, 61]. Resveratrol, a known NF-κB inhibitor, has been demonstrated to show neuroprotection against cerebral ischemia through enhancing autophagy [62]. In current study, autophagy markers LC3B1 and 2, beclin levels were upregulated in the CCH mice administered with IMS-088. An enhancement of autophagy by IMS-088 in the CCH mice likely promoted the clearance of insoluble phospho-TDP-43 aggregates.

Various studies reported that CCH can cause neuronal loss [63–66]. Activation of caspase-3 followed by proteolytic cleavage to yield cleaved caspase-3 is one of the important steps in apoptotic cell death process [67, 68]. Interestingly, treatment with IMS-088 significantly reduced cleaved caspase-3 levels after CCH which is consistent with its anti-apoptotic properties. Another possible factor for the reduction in cell death in the IMS-088-treated CCH mice could be linked to its effects on TDP-43-mediated pathology. A recent report suggests that cerebral hypoperfusion is an early marker that is associated with spread of TDP-43 proteinopathies in diseases like ALS and FTLD [69]. We observed that following CCH, there was a nuclear to cytoplasmic shift in TDP-43 expression indicating mislocalization thereby predisposing the protein to aggregation. IMS-088 treatment was found to restore the distribution of TDP-43 to the nucleus in cortical neurons of CCH mice. Hence, IMS-088 treatment may provide protection by restoring nuclear TDP-43 function.

In conclusion, our results provide an important in vivo evidence of a link between CCH, vascular dementia, and TDP-43 proteinopathy. Administration of IMS-088, a withaferin A analog inhibitor of NF-κB signaling, conferred beneficial effects in a mouse model of dementia caused by CCH, which included reversal of motor and cognitive deficits. Remarkably, by enhancing autophagy, the treatment was also effective in restoring the nuclear/cytoplasmic ratio of TDP-43 which is altered in pathological conditions. Taken together, the results of our study strongly suggest that targeting autophagy and TDP-43 pathogenic inclusions may have a disease-modifying effect in dementia caused by chronic brain hypoperfusion.

Supplementary Information The online version contains supplementary material available at https://doi.org/10.1007/s13311-021-01015-8.

Acknowledgements We are grateful to Mélanie Lalancette-Hébert for great suggestions and figures design. We thank Daniel Wattier and Imstar Therapeutics for providing the withanolide IMS-088.

Required Author Forms Disclosure forms provided by the authors are available with the online version of this article.

Funding This work was funded by Canadian Consortium for Neurodegenerative Diseases and Aging (CCNA) (J.K.) and the Hudson Translational Grant (ALS Canada/Brain Canada) to JPJ&JK. SST is recipient of Scholarship (PhD level) from Alzheimer Society of Canada. JPJ hold Canada Research Chair in Neurodegeneration.

Declarations

Conflict of Interest Dr. Jean-Pierre Julien is the CSO and co-founder of Imstar which provided IMS-088 for this study.

References

1. Dubois MF, Hebert R. The incidence of vascular dementia in Canada: a comparison with Europe and East Asia. Neuroepidemiology 2001;20:179-87.
2. Roman GC. Vascular dementia revisited: diagnosis, pathogenesis, treatment, and prevention. Med Clin North Am 2002;86:477-99.
3. Valerio Romanini C, Dias Fiuza Ferreira E, Correia Bacarin C, Verussa MH, Weffort de Oliveira RM, Milani H. Neurohistological and behavioral changes following the four-vessel occlusion/internal carotid artery model of chronic cerebral hypoperfusion: comparison between normotensive and spontaneously hypertensive rats. Behav Brain Res 2013;252:214–21.
4. Lee JS, Im DS, An YS, Hong JM, Gwag BJ, Joo IS. Chronic cerebral hypoperfusion in a mouse model of Alzheimer's disease: an additional contributing factor of cognitive impairment. Neurosci Lett 2011;489:84-8.
5. Jian H, Yi-Fang W, Qi L, Xiao-Song H, Gui-Yun Z. Cerebral blood flow and metabolic changes in hippocampal regions of a modified rat model with chronic cerebral hypoperfusion. Acta Neurol Belg 2013;113:313-7.
6. Jing Z, Shi C, Zhu L, Xiang Y, Chen P, Xiong Z. Chronic cerebral hypoperfusion induces vascular plasticity and hemodynamics but also neuronal degeneration and cognitive impairment. J Cereb Blood Flow Metab 2015;35:1249-59.
7. Du SQ, Wang XR, Xiao LY, Tu JF, Zhu W, He T. Molecular Mechanisms of Vascular Dementia: What Can Be Learned from Animal Models of Chronic Cerebral Hypoperfusion? Mol Neurobiol 2017;54:3670-82.
8. Kandiah N, Chander RJ, Ng A, Wen MC, Cenina AR, Assam PN. Association between white matter hyperintensity and medial temporal atrophy at various stages of Alzheimer's disease. Eur J Neurol 2015;22:150-5.
9. Adibhatla RM, Hatcher JF. Phospholipase A(2), reactive oxygen species, and lipid peroxidation in CNS pathologies. BMB Rep 2008;41:560-7.
10. Urabe T. [Molecular mechanism and new protective strategy for ischemic white matter damages]. Rinsho Shinkeigaku 2012;52:908-10.
11. Strong MJ, Volkening K, Hammond R, Yang W, Strong W, Leystra-Lantz C. TDP43 is a human low molecular weight neurofilament (hNFL) mRNA-binding protein. Mol Cell Neurosci 2007;35:320-7.
12. Wang IF, Wu LS, Chang HY, Shen CK. TDP-43, the signature protein of FTLD-U, is a neuronal activity-responsive factor. J Neurochem 2008;105:797-806.
13. Buratti E. TDP-43 post-translational modifications in health and disease. Expert Opin Ther Targets 2018;22:279-93.

14. Arai T, Hasegawa M, Akiyama H, Ikeda K, Nonaka T, Mori H. TDP-43 is a component of ubiquitin-positive tau-negative inclusions in frontotemporal lobar degeneration and amyotrophic lateral sclerosis. Biochem Biophys Res Commun 2006;351:602-11.
15. Neumann M, Sampathu DM, Kwong LK, Truax AC, Micsenyi MC, Chou TT. Ubiquitinated TDP-43 in frontotemporal lobar degeneration and amyotrophic lateral sclerosis. Science 2006;314:130-3.
16. Chang XL, Tan MS, Tan L, Yu JT. The Role of TDP-43 in Alzheimer's Disease. Mol Neurobiol 2016;53:3349-59.
17. de Boer EMJ, Orie VK, Williams T, Baker MR, De Oliveira HM, Polvikoski T. TDP-43 proteinopathies: a new wave of neurodegenerative diseases. J Neurol Neurosurg Psychiatry 2020.
18. Thammisetty SS, Pedragosa J, Weng YC, Calon F, Planas A, Kriz J. Age-related deregulation of TDP-43 after stroke enhances NF-kappaB-mediated inflammation and neuronal damage. J Neuroinflammation 2018;15:312.
19. Grover A, Shandilya A, Punetha A, Bisaria VS, Sundar D. Inhibition of the NEMO/IKKbeta association complex formation, a novel mechanism associated with the NF-kappaB activation suppression by Withania somnifera's key metabolite withaferin A. BMC Genomics 2010;11:S25.
20. Jackson SS, Oberley C, Hooper CP, Grindle K, Wuerzberger-Davis S, Wolff J. Withaferin A disrupts ubiquitin-based NEMO reorganization induced by canonical NF-kappaB signaling. Exp Cell Res 2015;331:58-72.
21. Hooper C, Jackson SS, Coughlin EE, Coon JJ, Miyamoto S. Covalent modification of the NF-kappaB essential modulator (NEMO) by a chemical compound can regulate its ubiquitin binding properties in vitro. J Biol Chem 2014;289:33161-74.
22. Lalancette-Hebert M, Phaneuf D, Soucy G, Weng YC, Kriz J. Live imaging of Toll-like receptor 2 response in cerebral ischaemia reveals a role of olfactory bulb microglia as modulators of inflammation. Brain 2009;132:940-54.
23. Kim JH, Ko PW, Lee HW, Jeong JY, Lee MG, Kim JH. Astrocyte-derived lipocalin-2 mediates hippocampal damage and cognitive deficits in experimental models of vascular dementia. Glia 2017;65:1471-90.
24. Boutej H, Rahimian R, Thammisetty SS, Beland LC, Lalancette-Hebert M, Kriz J. Diverging mRNA and Protein Networks in Activated Microglia Reveal SRSF3 Suppresses Translation of Highly Upregulated Innate Immune Transcripts. Cell Rep 2017;21:3220-33.
25. Guillemin I, Becker M, Ociepka K, Friauf E, Nothwang HG. A subcellular prefractionation protocol for minute amounts of mammalian cell cultures and tissue. Proteomics 2005;5:35-45.
26. Wils H, Kleinberger G, Janssens J, Pereson S, Joris G, Cuijt I. TDP-43 transgenic mice develop spastic paralysis and neuronal inclusions characteristic of ALS and frontotemporal lobar degeneration. Proc Natl Acad Sci U S A 2010;107:3858-63.
27. Pozzi S, Thammisetty SS, Julien JP. Chronic Administration of Pimozide Fails to Attenuate Motor and Pathological Deficits in Two Mouse Models of Amyotrophic Lateral Sclerosis. Neurotherapeutics 2018;15:715-727.
28. Swarup V, Phaneuf D, Bareil C, Robertson J, Rouleau GA, Kriz J. Pathological hallmarks of amyotrophic lateral sclerosis/frontotemporal lobar degeneration in transgenic mice produced with TDP-43 genomic fragments. Brain 2011;134:2610-26.
29. Dutta K, Patel P, Rahimian R, Phaneuf D, Julien JP. Withania somnifera Reverses Transactive Response DNA Binding Protein 43 Proteinopathy in a Mouse Model of Amyotrophic Lateral Sclerosis/Frontotemporal Lobar Degeneration. Neurotherapeutics 2017;14:447-62.
30. Lee Y, Oliynyk S, Jung JC, Han JJ, Oh S. Administration of glucosylceramide ameliorated the memory impairment in aged mice. Evid Based Complement Alternat Med 2013:824120.
31. Antunes M, Biala G. The novel object recognition memory: neurobiology, test procedure, and its modifications. Cogn Process 2012;13:93-110.
32. Aartsma-Rus A, van Putten M. Assessing functional performance in the mdx mouse model. J Vis Exp 2014(85).
33. Rommelfanger KS, Edwards GL, Freeman KG, Liles LC, Miller GW, Weinshenker D. Norepinephrine loss produces more profound motor deficits than MPTP treatment in mice. Proc Natl Acad Sci U S A 2007;104:13804-9.
34. Shindo A, Yata K, Sasaki R, Tomimoto H. Chronic cerebral ischemia induces redistribution and abnormal phosphorylation of transactivation-responsive DNA-binding protein-43 in mice. Brain Res 2013;1533:131-40.
35. Qiu L, Ng G, Tan EK, Liao P, Kandiah N, Zeng L. Chronic cerebral hypoperfusion enhances Tau hyperphosphorylation and reduces autophagy in Alzheimer's disease mice. Sci Rep 2016;6:23964.
36. Hasegawa M, Arai T, Nonaka T, Kametani F, Yoshida M, Hashizume Y. Phosphorylated TDP-43 in frontotemporal lobar degeneration and amyotrophic lateral sclerosis. Ann Neurol 2008;64:60-70.
37. Hossmann KA. Cerebral ischemia: models, methods and outcomes. Neuropharmacology 2008;55:257-70.
38. Hossmann KA. The two pathophysiologies of focal brain ischemia: implications for translational stroke research. J Cereb Blood Flow Metab 2012;32:1310-6.
39. Guedes ACB, Santin R, Costa ASR, Reiter KC, Hilbig A, Fernandez LL. Distinct Phospho-TDP-43 brain distribution in two cases of FTD, one associated with ALS. Dement Neuropsychol 2017;11:249-54.
40. Duncombe J, Kitamura A, Hase Y, Ihara M, Kalaria RN, Horsburgh K. Chronic cerebral hypoperfusion: a key mechanism leading to vascular cognitive impairment and dementia. Closing the translational gap between rodent models and human vascular cognitive impairment and dementia. Clin Sci (Lond) 2017;131:2451–68.
41. Yang Z, Zhang N, Shen H, Lin C, Lin L, Yuan B. Microglial activation with reduction in autophagy limits white matter lesions and improves cognitive defects during cerebral hypoperfusion. Curr Neurovasc Res 2014;11:223-9.
42. Tsai TH, Sun CK, Su CH, Sung PH, Chua S, Zhen YY, et al. Sitagliptin attenuated brain damage and cognitive impairment in mice with chronic cerebral hypo-perfusion through suppressing oxidative stress and inflammatory reaction. J Hypertens. 2015;33:1001-13.
43. Picher-Martel V, Dutta K, Phaneuf D, Sobue G, Julien JP. Ubiquilin-2 drives NF-kappaB activity and cytosolic TDP-43 aggregation in neuronal cells. Mol Brain 2015;8:71.
44. Patel P, Julien JP, Kriz J. Early-stage treatment with Withaferin A reduces levels of misfolded superoxide dismutase 1 and extends lifespan in a mouse model of amyotrophic lateral sclerosis. Neurotherapeutics 2015;12:217-33.
45. Walker AK, Spiller KJ, Ge G, Zheng A, Xu Y, Zhou M. Functional recovery in new mouse models of ALS/FTLD after clearance of pathological cytoplasmic TDP-43. Acta Neuropathol 2015;130:643-60.
46. O'Brien JT, Thomas A. Vascular dementia. Lancet 2015; 386(10004):1698-706.
47. Igaz LM, Kwong LK, Lee EB, Chen-Plotkin A, Swanson E, Unger T. Dysregulation of the ALS-associated gene TDP-43 leads to neuronal death and degeneration in mice. J Clin Invest 2011;121:726-38.
48. Swarup V, Phaneuf D, Dupre N, Petri S, Strong M, Kriz J. Deregulation of TDP-43 in amyotrophic lateral sclerosis triggers nuclear factor kappaB-mediated pathogenic pathways. J Exp Med 2011;208:2429-47.

49. Zhao W, Beers DR, Bell S, Wang J, Wen S, Baloh RH. TDP-43 activates microglia through NF-kappaB and NLRP3 inflammasome. Exp Neurol 2015;273:24-35.
50. Ohta Y, Tremblay C, Schneider JA, Bennett DA, Calon F, Julien JP. Interaction of transactive response DNA binding protein 43 with nuclear factor kappaB in mild cognitive impairment with episodic memory deficits. Acta Neuropathol Commun 2014;2:37.
51. Dutta K, Thammisetty SS, Boutej H, Bareil C, Julien JP. Mitigation of ALS pathology by neuron-specific inhibition of nuclear factor kappa B signaling. J Neurosci 2020;40:5137-5154.
52. Kaileh M, Vanden Berghe W, Heyerick A, Horion J, Piette J, Libert C. Withaferin a strongly elicits IkappaB kinase beta hyperphosphorylation concomitant with potent inhibition of its kinase activity. J Biol Chem 2007;282:4253-64.
53. Kumar S, Phaneuf D, Julien JP. Withaferin-A Treatment Alleviates TAR DNA-Binding Protein-43 Pathology and Improves Cognitive Function in a Mouse Model of FTLD. Neurotherapeutics : the journal of the American Society for Experimental NeuroTherapeutics 2020.
54. de la Torre JC. Are Major Dementias Triggered by Poor Blood Flow to the Brain? Theoretical Considerations. J Alzheimers Dis 2017;57:353-71.
55. Son JH, Shim JH, Kim KH, Ha JY, Han JY. Neuronal autophagy and neurodegenerative diseases. Exp Mol Med 2012;44:89-98.
56. Komatsu M, Waguri S, Chiba T, Murata S, Iwata J, Tanida I. Loss of autophagy in the central nervous system causes neurodegeneration in mice. Nature 2006;441:880-4.
57. Morimoto N, Oida Y, Shimazawa M, Miura M, Kudo T, Imaizumi K. Involvement of endoplasmic reticulum stress after middle cerebral artery occlusion in mice. Neuroscience 2007;147:957-67.
58. Nakka VP, Gusain A, Raghubir R. Endoplasmic reticulum stress plays critical role in brain damage after cerebral ischemia/reperfusion in rats. Neurotox Res 2010;17:189-202.
59. Yang C, Zhang X, Gao J, Wang M, Yang Z. Arginine vasopressin ameliorates spatial learning impairments in chronic cerebral hypoperfusion via V1a receptor and autophagy signaling partially. Transl Psychiatry 2017;7:e1174.
60. Nishikawa Y, Okuzaki D, Fukushima K, Mukai S, Ohno S, Ozaki Y, et al. Withaferin A Induces Cell Death Selectively in Androgen-Independent Prostate Cancer Cells but Not in Normal Fibroblast Cells. PLoS One 2015;10:e0134137.
61. Djavaheri-Mergny M, Amelotti M, Mathieu J, Besancon F, Bauvy C, Souquere S. NF-kappaB activation represses tumor necrosis factor-alpha-induced autophagy. J Biol Chem 2006;281:30373-82.
62. Liu Y, Yang H, Jia G, Li L, Chen H, Bi J. The Synergistic Neuroprotective Effects of Combined Rosuvastatin and Resveratrol Pretreatment against Cerebral Ischemia/Reperfusion Injury. J Stroke Cerebrovasc Dis 2018;27:1697-704.
63. Cechetti F, Pagnussat AS, Worm PV, Elsner VR, Ben J, da Costa MS. Chronic brain hypoperfusion causes early glial activation and neuronal death, and subsequent long-term memory impairment. Brain Res Bull 2012;87:109-16.
64. Soria G, Tudela R, Marquez-Martin A, Camon L, Batalle D, Munoz-Moreno E. The ins and outs of the BCCAo model for chronic hypoperfusion: a multimodal and longitudinal MRI approach. PLoS One 2013;8:e74631.
65. Wakita H, Tomimoto H, Akiguchi I, Matsuo A, Lin JX, Ihara M. Axonal damage and demyelination in the white matter after chronic cerebral hypoperfusion in the rat. Brain Res 2002;924:63-70.
66. Liu Z, Hu M, Lu P, Wang H, Qi Q, Xu J. Cerebrolysin alleviates cognitive deficits induced by chronic cerebral hypoperfusion by increasing the levels of plasticity-related proteins and decreasing the levels of apoptosis-related proteins in the rat hippocampus. Neurosci Lett 2017;651:72-8.
67. Polverino AJ, Patterson SD. Selective activation of caspases during apoptotic induction in HL-60 cells. Effects Of a tetrapeptide inhibitor. J Biol Chem 1997;272:7013–21.
68. Zhao Y, Zeng Y, Wu A, Yu C, Tang Y, Wang X. Lychee Seed Fraction Inhibits Abeta(1-42)-Induced Neuroinflammation in BV-2 Cells via NF-kappaB Signaling Pathway. Front Pharmacol 2018;9:380.
69. Ferraro PM, Jester C, Olm CA, Placek K, Agosta F, Elman L. Perfusion alterations converge with patterns of pathological spread in transactive response DNA-binding protein 43 proteinopathies. Neurobiol Aging 2018;68:85-92.